Generation of sub-half-wavelength micro-optical traps by dichroic evanescent standing waves

2007 Chinese Phys. 16 1295

(http://iopscience.iop.org/1009-1963/16/5/022)

Vol 16 No 5, May 2007
1009-1963/2007/16(05)/1295-05

Chinese Physics

Generation of sub-half-wavelength micro-optical traps by dichroic evanescent standing waves*

Zhang Jing(张 静), Zhang Tian-Cai(张天才)†,
Wang Jun-Min(王军民), and Peng Kun-Chi(彭堃墀)

State Key Laboratory of Quantum Optics and Quantum Optics Devices, Institute of Opto-Electronics, Shanxi University, Taiyuan 030006, *China*

(Received 10 March 2005; revised manuscript received 23 November 2006)

The bi-dimensional optical lattices formed by several sets of laser evanescent standing waves propagating at the surface of a dielectric prism are investigated. The characteristics of the optical traps including their depths and the sizes are analysed. It is shown that the micro-optical lattice with a sub-half-wavelength size can be achieved by the interference of the selected evanescent waves. The scheme together with the recently developed atomic chip may be used for atomic quantum manipulation.

Keywords: evanescent wave, optical dipole trap
PACC: 3280P, 3380P, 4250

1. Introduction

Many different schemes for trapping ultracold atoms have been demonstrated in the last decade. Of them, the optical dipole trap (ODT)[1] requires no magnetic fields and relatively few optical excitations to provide a truly conservative and tightly confining trapping potential, thus the ODT as an elegant and simple way to store laser-cooled neutral atoms has rapidly aroused the interest of all in recent years.[2−4] Far-off-resonance traps (FORT)[5] can confine atoms in all ground states for a long time with a very small ground-state relaxation rate.[6] All-optical Bose–Einstein condensation has been achieved.[7−9] In some cases, such as in cavity quantum electrodynamics,[10] it is of interest to use perfectly controlled or deterministic samples of atoms for further experiments involving quantum manipulation of exactly known number of atoms. The nearly conservative potential of ODT with a very low photon scattering rate offers the possibility of quantum manipulation. The full control of all internal and external atomic degrees of freedom is necessary in such applications.

Building small optical lattices is an effective method to strongly confine a few atoms. Several research groups have demonstrated a single-atom trap in experiment.[11−13] Through the elaborate optical designing, one has realized a tightly focused single Gaussian laser beam in free space with a beam waist that reaches the diffraction limit of light wavelength, and the optical traps with sub-micrometre size have been obtained.[14,15]

By using the standing waves formed inside an optical cavity one can obtain optical lattices with the size of each potential of half-wavelength. But further reducing the size of ODT is still a challenge. The diffraction limit prevents us from achieving the micro-traps with the size smaller than half-wavelength of the FORT beam, and the real confinement of an atom is still an open problem, especially when a long wavelength FORT beam is used in experiment.

The method of using evanescent light waves to control atoms was suggested in 1980s.[16] Double-wave evanescent atomic trap[17] and the loading process of the atoms in a Morse potential have been also investigated[18] and such a double-evanescent-wave-trapping scheme has already been realized experimentally.[19] But all these discussions are based on the evanescent running waves. In the present paper, we focus our study on the optical lattices that are formed by evanescent standing waves, instead of running waves of the medium. The formed optical lattices are different from the usual lattices formed in an empty optical cavity, and the configuration is also different from the above-mentioned systems[16−19] since

*Project supported by the National Natural Science Foundation of China (Grant Nos 10434080 and 60578018), the National Basic Research Program of China (Grant No 2006CB921102) and also by the CFKSTIP (705010) and PCSIRT (IRT0516) from MEC.
†E-mail: tczhang@sxu.edu.cn

no optical lattice can be built up by evanescent running waves. It is the first time that optical dipole traps with sub-half-wavelength size have been obtained on the surface of a dielectric medium by four sets of evanescent standing waves (totally eight beams) tuned at appropriate wavelengths. The van der Waals potential is also considered and it clearly shows that the distinctive features of such a scheme lie in the formation of sub-half-wavelength controllable potential traps which may provide a better confinement and control of the atoms.

2. Theoretical model

The basic geometrical configuration is shown in Fig.1. First we consider two beams of plane light waves propagating in opposite directions at the same frequency ω_1 and same incident angle θ_1 from the medium whose refraction index is n to vacuum. The coordinates are shown in Fig.1. If θ_1 is larger than a critical angle, the light will be totally reflected and the two evanescent waves $\tilde{E}_2$ and $\tilde{E}_2'$ propagating in opposite directions in the vacuum near the surface are generated[20] as follows

$$\tilde{E}_2 = E_2 \mathrm{e}^{-\frac{\omega_1}{c} z\sqrt{n^2\sin^2\theta_1 - 1}} \mathrm{e}^{\mathrm{i}\left(\frac{\omega_1 n}{c}\sin\theta_1 x - \omega_1 t\right)}, \quad (1)$$

$$\tilde{E}_2' = E_2 \mathrm{e}^{-\frac{\omega_1}{c} z\sqrt{n^2\sin^2\theta_1 - 1}} \mathrm{e}^{\mathrm{i}\left(-\frac{\omega_1 n}{c}\sin\theta_1 x - \omega_1 t\right)}, \quad (2)$$

where E_2 is the amplitude of initial field entering the prism.

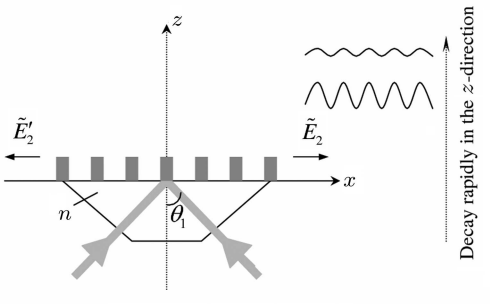

Fig.1. Two-beam configuration.

The evanescent waves, $\tilde{E}_2$ and $\tilde{E}_2'$, are running-waves in the x-direction along the interface, and their amplitudes decay rapidly in the z-direction (vertical direction). In the overlapped range of two evanescent waves at the surface, a stable intensity distribution is built up through the interference

$$I = 2|E_2|^2 \mathrm{e}^{-\frac{2\omega_1}{c} z\sqrt{n^2\sin^2\theta_1 - 1}} \left[1 + \cos\left(\frac{2\omega_1 n\sin\theta_1}{c} x\right)\right]. \quad (3)$$

The one-dimensional standing-light field is then formed under certain conditions, and the size of each potential is the distance between two adjacent antinodes,

$$d = \frac{\lambda_1}{2n\sin\theta_1}, \quad (4)$$

where λ_1 is the wavelength of incident beams. It is seen from the expression (4) that the size of the potential depends on the index and the incident angle. A higher refraction index and larger incident angle lead to a smaller lattice.

In the case of Gaussian beams, the intensities of the incident light teams I_1 and I_2 can be expressed as follows:

$$I_1 = I(x', y, z') = \frac{2P}{\pi\omega^2(x')} \exp\left[-2\frac{y^2 + z'^2}{\omega^2(x')}\right], \quad (5)$$

where $x' = x\sin\theta_1 + z\cos\theta_1$ and $z' = -x\cos\theta_1 + z\sin\theta_1$, and

$$I_2 = I(x'', y, z'') = \frac{2P}{\pi\omega^2(x'')} \exp\left[-2\frac{y^2 + z''^2}{\omega^2(x'')}\right], \quad (6)$$

where $x'' = -x\sin\theta_1 + z\cos\theta_1$ and $z'' = -x\cos\theta_1 - z\sin\theta_1$. P is the incident power. Here we have considered that the incident Gaussian beams are not along the x-direction, and coordinate transformations have been made.

The evanescent waves then take the forms

$$\tilde{E}_1 = E_1 \mathrm{e}^{-\frac{\omega_1}{c} z\sqrt{n^2\sin^2\theta_1 - 1}} \mathrm{e}^{\mathrm{i}\left(\frac{\omega_1 n}{c}\sin\theta_1 x - \omega_1 t\right)}, \quad (7)$$

and

$$\tilde{E}_2 = E_2 \mathrm{e}^{-\frac{\omega_1}{c} z\sqrt{n^2\sin^2\theta_1 - 1}} \mathrm{e}^{\mathrm{i}\left(-\frac{\omega_1 n}{c}\sin\theta_1 x - \omega_1 t\right)}, \quad (8)$$

where $E_1^2 = \dfrac{2c\mu_0}{n} I_1$ and $E_2^2 = \dfrac{2c\mu_0}{n} I_2$. E_1 and E_2 are the amplitudes of initial fields entering the prism. The total intensity distribution superposed by the two evanescent waves is then

$$I_\mathrm{t} = \frac{1}{n}\mathrm{e}^{-\frac{2\omega_1}{c} z\sqrt{n^2\sin^2\theta_1 - 1}} \Big[I_1 + I_2 + 2\sqrt{I_1 I_2}\cos\left(\frac{2\omega_1 n}{c}\sin\theta_1 x\right)\Big]. \quad (9)$$

Add up two beams the same as the above beams but in the y–z plane, as shown in Fig.2. The intensity distribution of I_t' of these two evanescent waves in the y-direction has a similar form to the expression (9), with x simply replaced with y in the expression (9).

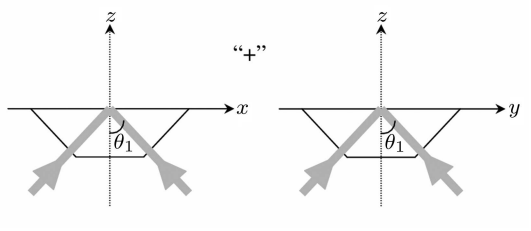

Fig.2. Four-beam configuration. Two beams are in the x–z plane and another two in the y–z plane.

The optical dipole potential $U_{\rm dip}$ is closely related to the light intensity. Under certain conditions, we have[4]

$$U_{\rm dip} = \frac{\hbar\Gamma^2}{8I_{\rm s}} \frac{I_{\rm t} + I'_{\rm t}}{\omega_1 - \omega_{\rm a}}, \tag{10}$$

where Γ and $\omega_{\rm a}$ are the natural line-width and the resonance frequency of the corresponding atomic transition, respectively. ω_1 is the frequency of the incident laser beam. The trap depth can be also expressed in units of temperature T as follows:

$$T = \frac{U_{\rm dip}}{k_{\rm B}}, \tag{11}$$

where $k_{\rm B}$ is the Boltzmann constant.

Clearly, the optical lattices can be achieved by gradient light field on the surface, and the size of each potential can be reduced either by using those mediums with a large refraction index or by increasing the incident angle.

We further consider the dichroic-trap which is formed by two sets of red and blue-detuned beams simultaneously[20] as shown in Fig.3. A set of four blue-detuned beams incident upon the prism at a larger incident angle θ_2 than that of the red-detuned beams.

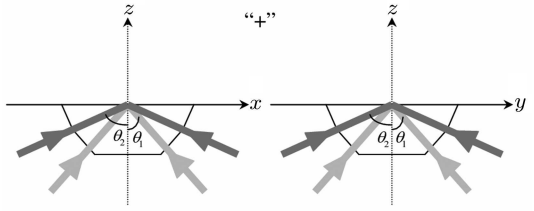

Fig.3. The configuration of dichroic cross traps. The grey lines represent red detuned beams at an incident angle θ_1, and black lines the blue detuned beams at an incident angle θ_2. The beams in the x–z plane and y–z plane are symmetric.

Similarly, we can obtain the light intensity distributions of the blue-detuned beams $I''_{\rm t}$ and $I'''_{\rm t}$, corresponding to the two sets of beams in the x–z and y–z planes, respectively, which are similar to Eq.(10), just with λ_1, θ_1, ω_1 replaced by λ_2, θ_2, ω_2, $I_{\rm t}$ and $I'_{\rm t}$ by $I''_{\rm t}$ and $I'''_{\rm t}$, respectively. The red-detuned beams tend to pull the atom toward the surface of the prism while the blue-detuned beams to push it away from the surface, and the atom can be trapped at an appropriate distant from the surface.

The optical dipole potential of the dichroic cross trap is given by[17]

$$U_{\rm dip} = \frac{\hbar\Gamma^2}{8I_{\rm s}} \left(\frac{I_{\rm t} + I'_{\rm t}}{\omega_1 - \omega_{\rm a}} + \frac{I''_{\rm t} + I'''_{\rm t}}{\omega_2 - \omega_{\rm a}} \right), \tag{12}$$

where $I_{\rm s}$ is the atomic saturation intensity.

The van der Waals potential between atoms and the molecules at a medium surface takes the form[21]

$$U_{\rm vdw}(z) = -\frac{\varepsilon - 1}{\varepsilon + 1} \frac{1}{48\pi\varepsilon_0} \frac{D^2}{z^3}, \tag{13}$$

where ε is the dielectric coefficient and ε_0 the vacuum dielectric coefficient, D the transition dipole matrix element corresponding to the atom. Then, the total potential is

$$T = (U_{\rm dip} + U_{\rm vdw})/k_{\rm B}. \tag{14}$$

3. Numerical results and analysis

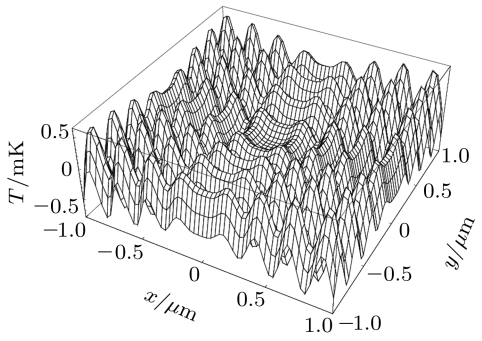

Fig.4. Dichroic cross traps in the x–y plane at $z = 165$ nm. Atom saturation intensity $I_{\rm s} = 2.70\,{\rm mW/cm^2}$; dipole matrix element of D_2 line $D = 3.797 \times 10^{-29}{\rm C{\cdot}m}$; Dielectric coefficient ε for the material is 7.4. All other parameters are shown in context.

We discuss the caesium atom for simulation and choose the D_2 line ($\lambda_{\rm a} = 852.3\,{\rm nm}$) without losing the generality. The natural line-width $\Gamma/2\pi = 5.2\,{\rm MHz}$. We select the wavelengths of blue and red-detuned beams to be $\lambda_1 = 857.3\,{\rm nm}$ and $\lambda_2 = 850\,{\rm nm}$, respectively. Each beam has a power of 600 mW and the beam radius is $20\,\mu{\rm m}$. The material is assumed to have

a refraction index of 1.9, such as the material of dense flint glass, and its critical angle is 31.7 degrees accordingly. The incident angle of the red-detuned beams is 60 degrees, whereas 80 degrees for the blue-detuned beams. Figure 4 shows the 3D map of the traps in the x–y plane within an area of 4 square micrometres according to Eq.(4), where the van der Waals potential has been considered. We can see that the distribution of the lattices on the surface is not homogeneous for both the space and the depth of the optical potential wells in the area around the central point of $x = 0$ and $y = 0$.

Now we take a close look at the magnified individual trap. Figure 5 shows two typical trap in the lattice at $x = 0$ and $y = 0$ (Fig.5(a)) and $x = 0.31\,\mu$m and $y = 0.31\,\mu$m (Fig.5(b)). The sizes of the two traps are of $0.4\,\mu$m and $0.26\,\mu$m, respectively, and both are less than half-wavelength of the FORT beams.

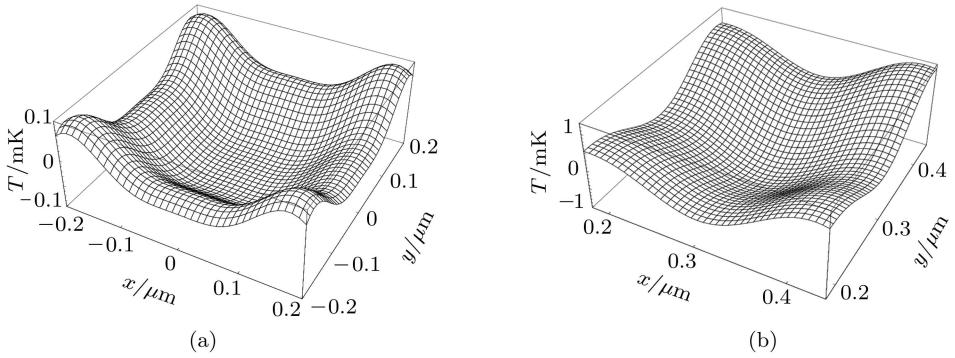

Fig.5. Two magnified typical traps in Fig.4 at $x = y = 0\,\mu$m (a), and $x = y = 0.31\,\mu$m (b).

We investigate the depth of the potential. Figure 6 shows the potential depth as a function of vertical distance z with different powers at two points $x = y = 0$ and $x = y = 0.26\,\mu$m. Higher power is helpful to obtain a deeper trap-depth. The minimum potentials appear here at about $z = 165$ nm and 105 nm for the two traps at which positions the van der Waals interaction does contribute to the potential as discussed below. About 1 mK of the potential depth can be achieved with a few watts of laser team in power that can be reached in experiment. The atoms pre-cooled by a general magneto-optical trap (MOT) can be loaded into this lattice, and the strong confinement of atom can be realized.

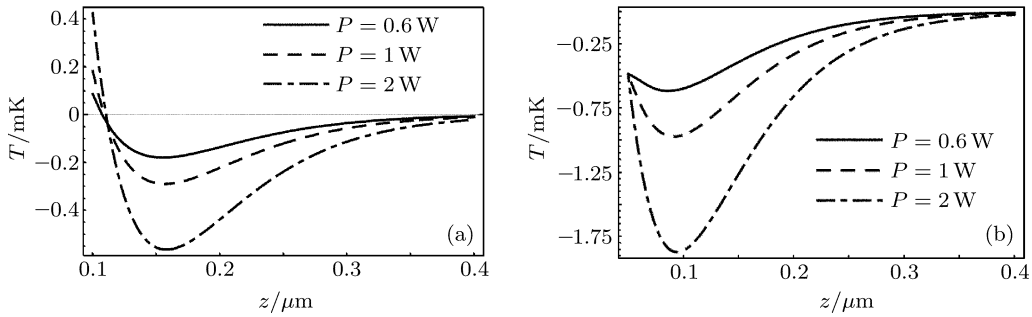

Fig.6. Potential depth as a function of vertical distance z for different powers at points $x = y = 0$ (a), and $x = y = 0.26\,\mu$m (b).

Figure 7 shows the difference between with and without considering the van der Waals potential based on the dichroic cross configuration at the points of $x = y = 0$ and $x = y = 0.26\,\mu$m, respectively. The solid line represents the result with considering the van der Waals potential whereas the dashed line is for the results without considering it. Clearly the van der Waals potential changes the dichroic cross potential. Generally, it increases the minimum potential depth, especially in the range where the minimum potential point is closer to the surface.

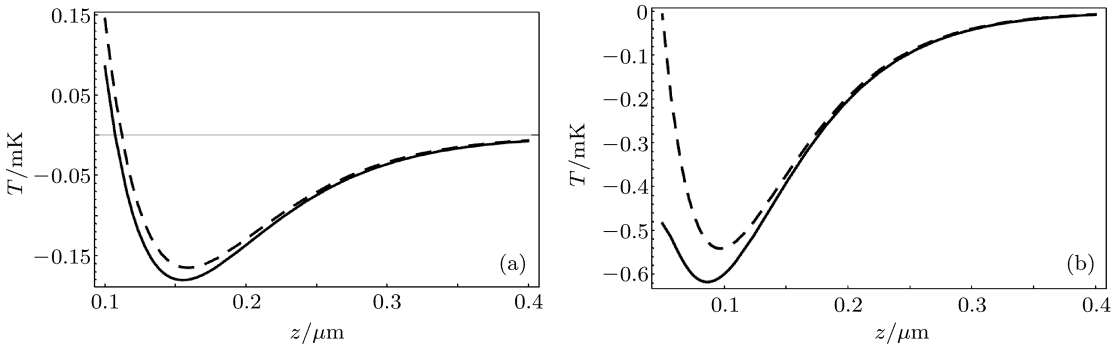

Fig.7. The potential depths with (solid lines) and without (dashed line) considering the van der Waals interaction. The laser beam power is 0.6 W. (a) $x = y = 0$; (b) $x = y = 0.26\,\mu$m. Other parameters are the same as those in Fig.6.

Usually the scattering rate should be taken into consideration. By using the formula

$$\Gamma_{\rm SC}(r) = \frac{3\pi c^2}{2\hbar\omega_{\rm a}^3}\left(\frac{\Gamma}{\Delta}\right)^2 I(r), \qquad (15)$$

the scattering rate under the above condition can be obtained. The scattering rates are 2 photons/ms (for red-detuned case) and 10 photons /ms (for blue-detuned case), which are very smaller than those under the resonant condition. And we can make them lower by modifying the wavelength of the incident light. For example, if 882 nm and 840 nm are chosen to be the wavelengths of the incident light, then the scattering rate will be 64 photons/s (for red-detuned case) and 360 photons/s (for blue-detuned case). Comparing with the recent result presented by the D-Meschede group in Germany (laser of 1064 nm and 8–10 W, detuning to Cs atom D_2 line, trapping single atom for 20–40 s), the scheme that we mentioned above is feasible indeed.

4. Conclusions

We have discussed the sub-half-wavelength micro-traps generated by using several evanescent light waves based on a dichroic cross configuration. The size of the lattice cell is determined basically by $\lambda/(2n\sin\theta)$ which is much less than half-wavelength of the FORT beams. With a few watts of the laser beams in power, an optical lattice with a potential depth of around 1mK can be achieved, and the pre-cooled atoms from MOT can be loaded into such traps and strongly confined. Together with the newly developed atom chip, this method may be used to manipulate individual atoms.

References

[1] Chu S, Bjorkholm J E, Ashkin A and Cable A 1986 *Phys. Rev. Lett.* **57** 314

[2] Gordon J P and Ashkin A 1980 *Phys. Rev.* A **21** 1606

[3] Kuppens S J M, Corwin K L, Miller K W, Chupp T E and Wieman C E 2000 *Phys. Rev.* A **62** 013406

[4] Weidemuller M and Ovchinnikov Y B 2000 *Adv. At. Mot. Opt. Phys.* **42** 95

[5] Miller J D, Cline R A and Heinzen D J 1993 *Phys. Rev.* A **47** 4567

[6] Cline R A, Miller J D, Matthews M R and Heinzen D J 1994 *Opt. Lett.* **19** 207

[7] Barrett M D, Sauer J A and Chapman M S 2001 *Phys. Rev. Lett.* **87** 010404

[8] Weber T, Herbig J, Mark M, Nägerl H C and Grimm R 2003 *Science* **299** 232

[9] Yosuke Takasu, Kenichi Maki, Kaduki Komori, Tetsushi Takano, Kazuhito Honda and Mitsutaka Kumakura 2003 *Phys. Rev. Lett.* **91** 040404

[10] Berman P R 1994 *Cavity Quantum Electrodynamics* (San Diego: Academic)

[11] Ye J, Vernooy D W and Kimble H J 1999 *Phys. Rev. Lett.* **83** 4987

[12] Hood C J, Lynn T W, Doherty A C, Parkins A S and Kimble H J 2000 *Science* **287** 1447

[13] Pinkse P W H, Fischer T, Maunz P and Rempe G 2000 *Nature* **404** 365

[14] Frese D, Ueberholz B, Kuhr S, Alt W, Schrader D, Gomer V and Meschede D 2000 *Phys. Rev. Lett.* **85** 3777

[15] Nicolas S, Reymond G, Protsenko I and Grangier P 2001 *Nature* **411** 1024

[16] Cook R J and Hill R K 1982 *Opt. Commun.* **43** 258

[17] Ovchinnikov Y B, Shul'ga S V and Balykin V I 1991 *J. Phys.* B **24** 3137

[18] Desbiolles P and Dalibard J 1996 *Opt. Commun.* **132** 540

[19] Hammes M, Rychtarik D, Engeser B, Nägerl H C and Grimm R 2003 *Phys. Rev. Lett.* **90** 173001

[20] Born M and Wolf E 1999 *Principles of Optics* Seventh Edition (Cambridge: Cambridge University Press) p50

[21] Landragin A, Courtois J Y, Labeyrie G, Vansteenkiste N, Westbrook C I and Aspect A 1996 *Phys. Rev. Lett.* **77** 1464